LETTER

doi:10.1038/nature19756

Clock–driven vasopressin neurotransmission mediates anticipatory thirst prior to sleep

C. Gizowski[1], C. Zaelzer[1] & C. W. Bourque[1]

Circadian rhythms have evolved to anticipate and adapt animals to the constraints of the earth's 24-hour light cycle[1]. Although the molecular processes that establish periodicity in clock neurons of the suprachiasmatic nucleus (SCN) are well understood, the mechanisms by which axonal projections from the central clock drive behavioural rhythms are unknown[2–4]. Here we show that the sleep period in mice (Zeitgeber time, ZT0–12) is preceded by an increase in water intake promoted entirely by the central clock, and not motivated by physiological need. Mice denied this surge experienced significant dehydration near the end of the sleep period, indicating that this water intake contributes to the maintenance of overnight hydromineral balance. Furthermore, this effect relies specifically on the activity of SCN vasopressin (VP) neurons that project to thirst neurons in the OVLT (organum vasculosum lamina terminalis), where VP is released as a neurotransmitter. SCN VP neurons become electrically active during the anticipatory period (ZT21.5–23.5), and depolarize and excite OVLT neurons through the activation of postsynaptic VP V1a receptors and downstream non-selective cation channels. Optogenetic induction of VP release before the anticipatory period (basal period; ZT19.5–21.5) excited OVLT neurons and prompted a surge in water intake. Conversely, optogenetic inhibition of VP release during the anticipatory period inhibited the firing of OVLT neurons and prevented the corresponding increase in water intake. Our findings reveal the existence of anticipatory thirst, and demonstrate this behaviour to be driven by excitatory peptidergic neurotransmission mediated by VP release from central clock neurons.

Nocturnal rodents display a surge in water intake before sleep[5,6]; however, whether the clock mediates this behaviour and serves an anticipatory physiological benefit remains to be determined. We monitored water intake in wild-type mice and confirmed that water intake increased significantly during the anticipatory period (AP) compared to the basal period (BP; Fig. 1a, b). Increased water intake during the AP was not motivated by physiological stimuli for thirst, such as hyperosmolality[7], increased core body temperature[8], or hypovolaemia[9] (Fig. 1b). In addition, food restriction throughout the BP and AP did not prevent a significant increase in water intake during the AP ($P < 0.05$, $n = 8$, paired t-test, data not shown), indicating that increased water intake at this time does not simply reflect prandial drinking. These data suggest this behaviour is need-free and may be driven directly by the central clock. To test whether this behaviour is physiologically relevant, we investigated the effect of denying the water-intake surge during the AP on serum osmolality and haematocrit measured near the end of the light period (ZT10; Fig. 1c). Animals subjected to this procedure displayed a significantly elevated serum osmolality and haematocrit, indicating a state of dehydration (Fig. 1d). These data indicate that increased water intake during the AP mitigates the impact of reduced water intake during sleep, and therefore serves an important homeostatic function.

Previous work established that the OVLT critically regulates water intake in mammals[10–12] and that increased activity in this area orchestrates thirst perception in humans[13–15]. Owing to the circadian nature of AP water intake[16,17], we hypothesized that this behaviour relies on connections between the SCN and OVLT. In support of this hypothesis, cell-attached recordings in slices of mouse hypothalamus that retain both nuclei (Extended Data Figs 1, 2) revealed that the average firing rate and proportions of active OVLT neurons were significantly increased during the subjective AP compared to BP *in vitro* (Fig. 2a–c). Equivalent results were obtained in rat OVLT neurons (data not shown). In agreement with these observations, the density of OVLT neurons expressing c-Fos protein was increased during the AP compared to the BP in mice, providing *in vivo* support for increased

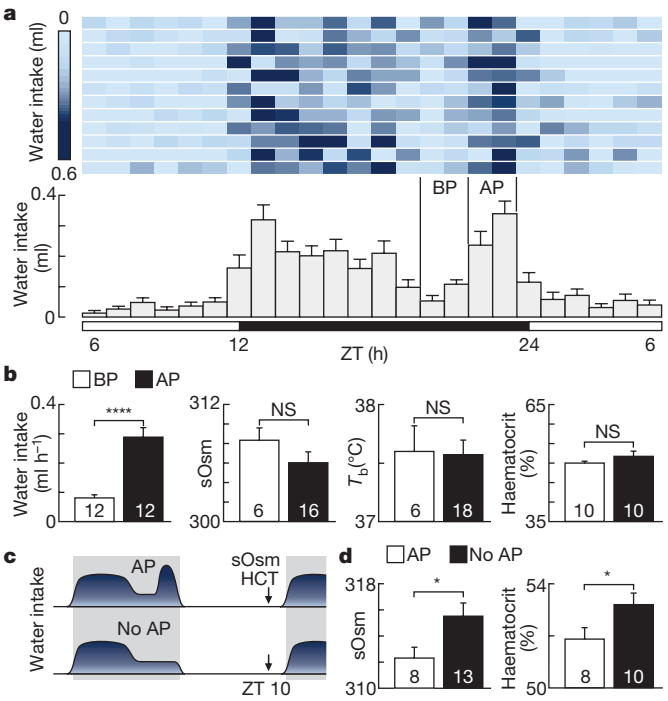

Figure 1 | Mice display anticipatory thirst during the AP. a, Raster plot shows daily water intake in 12 wild-type mice. Histogram plots mean ± s.e.m. water intake. **b**, Bar graphs compare water intake (****$P < 0.0001$, paired t-test) and physiological parameters during BP and AP (mean ± s.e.m.; serum osmolality, sOsm, t-test; core body temperature, T_b, t-test; volaemia, haematocrit, Mann–Whitney test; NS, $P > 0.05$). **c**, Schematic of protocol used to compare the impact of allowing (AP) or denying (No AP) water intake on serum osmolality and haematocrit at ZT10. **d**, Serum osmolality and haematocrit in mice subjected to protocol in **c** (mean ± s.e.m.; *$P < 0.05$, t-test). n as indicated.

[1]Centre for Research in Neuroscience and Brain Repair and Integrative Neuroscience Program, Research Institute of the McGill University Health Centre, 1650 Cedar Avenue, Montreal H3G 1A4, Canada.

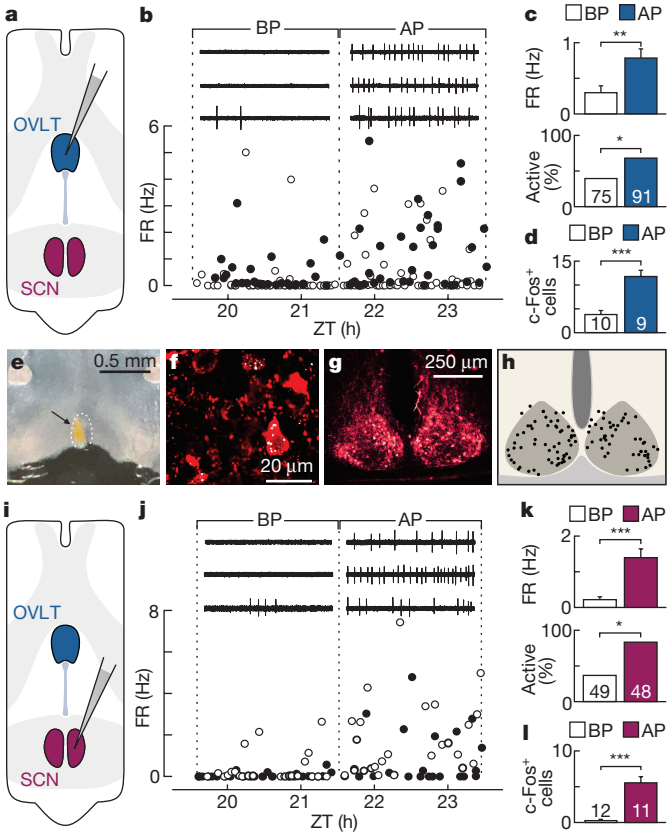

Figure 2 | OVLT and SCN VP neurons show increased activity during the AP. a, Schematic illustrating recording from OVLT neurons. **b**, Closed and opened circles plot firing rate (FR) of individual OVLT neurons in slices from ChETA and ArchT mice, respectively (5-s excerpts shown above). **c**, Plots show firing rate (mean ± s.e.m., Mann–Whitney test) and percentages of active cells (χ^2 test; $^*P < 0.05$, $^{**}P < 0.01$). **d**, Number of c-Fos$^+$ cells per section (mean ± s.e.m.; $^{***}P < 0.001$, Mann–Whitney test). **e**, Image of injection site (arrow) of microspheres into OVLT (dotted line). **f**, SCN VP neurons (red) containing microspheres (white). **g**, VP-labelled neurons in mouse SCN. **h**, Positions of VP neurons containing microspheres (total of 109 cells from three separate experiments). **i**, Schematic illustrating recording from SCN VP neurons. **j**, Closed and open circles plot firing rate of individual SCN VP neurons in slices from ChETA and ArchT mice, respectively (5-s excerpts shown above). **k**, Plots show firing rate (mean ± s.e.m., Mann–Whitney test) and percentages of active cells (χ^2 test). **l**, Number of c-Fos$^+$ SCN VP neurons (mean ± s.e.m., Mann–Whitney test). *n* as indicated.

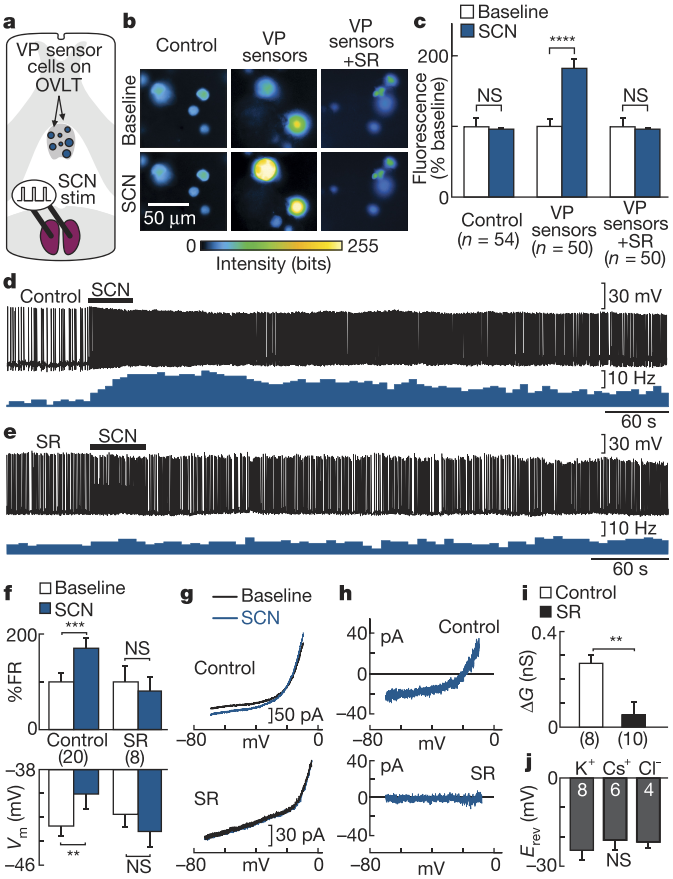

Figure 3 | VP released by SCN axon terminals excites OVLT neurons via non-selective cation channels. a, Schematic illustrating detection of SCN-mediated VP release in the rat OVLT. **b**, GCaMP6m fluorescence in HEK293 cells before (baseline) and after SCN stimulation (SCN; 40 s, 10 Hz). Control cells lack V1aR, VP sensors contain both GCaMP6m and V1aR, and VP sensors + SR are tested in the presence of SR49059 (10 µm). **c**, SCN stimulation-induced changes in fluorescence (mean ± s.e.m.; $^{****}P < 0.0001$; NS, $P > 0.05$; paired *t*-test). Similar results were obtained in mouse Extended Data Fig. 6). **d**, Voltage response of OVLT neuron to SCN stimulation (bar; 30 s, 10 Hz) in the presence of kynurenate (3 mM) and bicuculline (10 µm). Lower trace shows firing rate. **e**, Recording from an OVLT neuron in the presence of SR49059 (with kynurenate and bicuculline), layout as in **d**. **f**, Firing rate expressed as percentage of respective baseline (%FR) before and after SCN stimulation (30 s, 10 hz) without (control) or with SR49059 (mean ± s.e.m., paired *t*-test). Lower graph shows corresponding changes in membrane voltage (V_m; control, Wilcoxon test; SR, paired *t*-test; $^{**}P < 0.01$, $^{***}P < 0.001$). **g**, Steady-state current–voltage (I–V) relations in OVLT neurons before (baseline) and after (SCN) SCN stimulation in control conditions or with SR49059. **h**, Difference currents obtained from corresponding I–V curves in **g**. **i**, Mean ± s.e.m. change in membrane conductance (ΔG) caused by SCN stimulation in control conditions or with SR49059 ($^{**}P < 0.01$, Mann–Whitney test). **j**, Reversal potentials (E_{rev}) of SCN-induced currents measured with pipettes containing K^+, Cs^+, or high Cl^- solutions (mean ± s.e.m., one-way ANOVA). *n* as indicated.

neuronal activation (Fig. 2d). Anatomical studies have suggested that VP neurons in the shell of the SCN serve as major output cells of the clock[18–21]. We therefore investigated whether such neurons projected to the OVLT by injecting fluorescent microspheres into the OVLT (Fig. 2e and Extended Data Fig. 3). Confocal analysis of tissue sections obtained one week after injection revealed the presence of microspheres in VP neurons in the shell of the SCN (Fig. 2f–h), but not in other regions containing VP neurons (Extended Data Fig. 3). Thus, the VP-containing fibres in the OVLT specifically emanated from SCN VP neurons (Extended Data Fig. 4).

To determine whether the activity of SCN VP neurons increased during the AP, we obtained visually guided cell-attached recordings from these neurons in slices prepared from mice in which fluorescent reporters are driven by the VP promoter (Fig. 2i and Extended Data Fig. 4). The data revealed that the average firing rate and proportions of active SCN VP neurons were significantly increased during the AP compared to the BP (Fig. 2j, k). Equivalent results were obtained in rat hypothalamic slices (data not shown). In agreement with these *in vitro* data, the density of SCN VP neurons expressing c-Fos protein was increased during the AP compared to the BP *in vivo* (Fig. 2l).

The above findings suggest that the increased firing of OVLT neurons may rely on excitatory neurotransmission mediated by the increased activity of SCN VP neurons during the AP. To test whether VP is released within the OVLT, we examined the effects of SCN stimulation on the fluorescence of VP sensors plated over rat hypothalamic slices (Fig. 3a). These sensors consisted of HEK293 cells co-expressing the calcium indicator GCaMP6m[22] and the VP V1a receptor (V1aR), which together promoted a dose-dependent calcium response to

exogenous VP (Extended Data Fig. 5). Electrical stimulation of the SCN significantly increased fluorescence in cells containing V1aRs, but did not do so in the presence of the selective V1aR blocker, SR49059 (ref. 23) or in HEK293 cells lacking V1aRs (Fig. 3a–c). Importantly, stimulation-induced VP release was observed only in discrete regions of the slice (Extended Data Fig. 6), indicating that VP sensor activation over the OVLT did not result from volume transmission, but reflected local and activity-dependent release at this site.

We next investigated the effects of SCN stimulation on OVLT neurons using whole-cell voltage recordings. Electrical stimulation of the SCN (30 s at 10 Hz) caused reversible depolarization and excitation of OVLT neurons in either mouse or rat hypothalamic slices (data not shown). These effects persisted during blockade of ionotropic glutamate and γ-aminobutyric acid (GABA) receptors (Fig. 3d, f), supporting our hypothesis that OVLT neurons may be directly depolarized and excited by a postsynaptic action of VP itself. Single-cell RT–PCR revealed that OVLT neurons express V1aRs (Extended Data Fig. 7); therefore, we investigated whether such receptors mediated these excitatory effects. Indeed, the effects of SCN stimulation were abolished by SR49059 (Fig. 3e, f). Moreover, voltage-clamp analysis revealed that SCN stimulation caused a V1aR-dependent increase in membrane conductance associated with the appearance of an inward current that reversed near −25 mV (Fig. 3g–i). The reversal potential of the current was unaffected by changes in the intracellular concentrations of potassium or chloride ions (Fig. 3j), indicating that VP released by the axon terminals of SCN neurons excites OVLT neurons by V1aR-dependent activation of non-selective cation channels.

To determine whether the increased firing rate of OVLT neurons during the AP is caused by the SCN–OVLT projection, we examined the impact of manipulating VP release using optogenetic approaches in mice expressing excitatory E123T mutant channelrhodopsin 2 (ChETA)[24], or inhibitory archaerhodopsin-3 (ArchT)[25] driven by the VP promoter (Extended Data Figs 4, 8). Application of blue light (473 nm) over the OVLT in hypothalamic slices prepared from ChETA mice caused VP release as measured by VP sensors (Fig. 4a–c). In addition, blue light significantly increased the firing rate of OVLT neurons in ChETA preparations during the BP (Fig. 4d). Consistent with the involvement of VP release and V1aRs in this effect, the firing rate in the presence of blue light was significantly reduced by bath application of SR49059 (Fig. 4d), but was unaffected by the selective V1bR antagonist SSR149415 (ref. 26) (10 nM, $n = 24$, $P > 0.05$, Mann–Whitney test; data not shown). Conversely, activation of ArchT with yellow light (589 nm) reduced the firing of OVLT neurons during the AP, and this effect was occluded and mimicked by SR49059 (Fig. 4d). Taken together, these data support our hypothesis that increased OVLT firing during the AP is specifically dependent on postsynaptic V1aRs and VP release from the axon terminals of SCN VP neurons.

To further investigate the involvement of V1aRs in increasing the activity of OVLT neurons and water intake during the AP *in vivo*, additional experiments were performed on V1aR knockout ($V1aR^{-/-}$) mice. Although a rise in c-Fos expression was observed in SCN VP neurons of $V1aR^{-/-}$ mice during the AP (BP $n = 11$, AP $n = 12$, $P < 0.001$, Mann–Whitney test; data not shown), this effect was absent in OVLT neurons (Fig. 4e). $V1aR^{-/-}$ mice also failed to show an increase in water intake during the AP (Fig. 4f and Extended Data Fig. 7), indicating that V1aRs are necessary to activate OVLT neurons and generate this behaviour.

Finally, to determine whether increased water intake during the AP is driven by the central clock, we examined the effects of optogenetically regulating VP release *in vivo* via light delivery through an implanted fibre-optic cannula targeting the OVLT (Extended Data Fig. 9). As in wild-type mice, ChETA and ArchT mice that were implanted but not photostimulated displayed significant increases in water intake during the AP (Extended Data Fig. 10). Application of blue light to the OVLT, but not adjacent sites (Extended Data Fig. 9), in ChETA mice during the BP significantly increased water intake, whereas yellow light had no effect (Fig. 4g). Notably, water intake induced by blue light (0.50 ± 0.16 ml h^{-1}) was equivalent to that observed during the AP in implanted but unstimulated ChETA mice (0.43 ± 0.09 ml h^{-1}, $P > 0.05$, Mann–Whitney test; data not shown), suggesting that light-induced VP release is sufficient to cause a surge in water intake similar to that observed during the AP. Conversely, application of yellow light to the OVLT in ArchT mice abolished the water-intake surge observed during

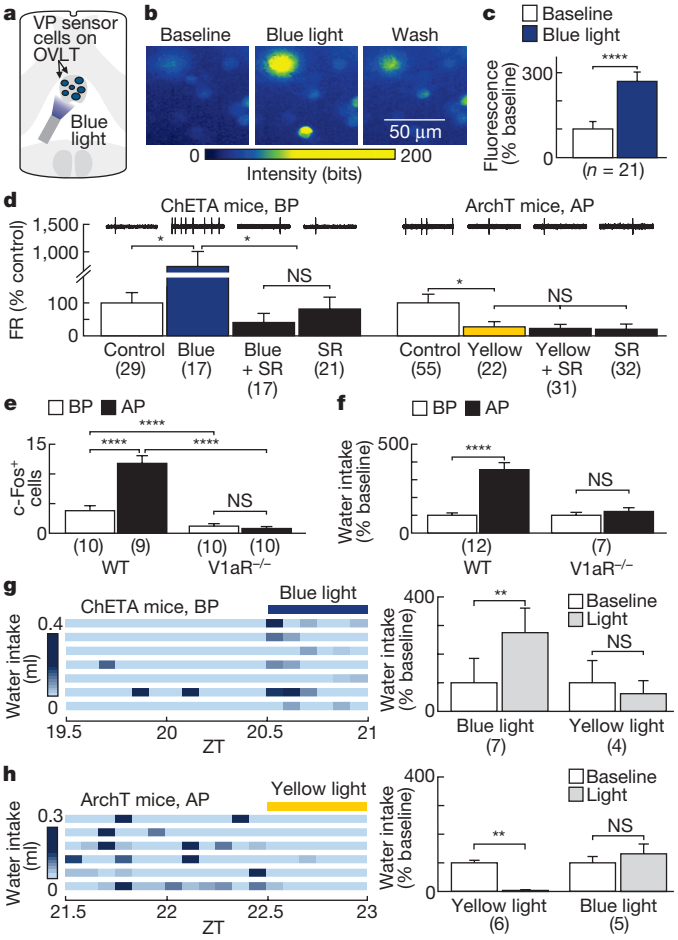

Figure 4 | Optogenetic and V1aR-dependent control of OVLT neuron firing and water intake. a, Schematic illustrating detection of light-mediated SCN VP release in the OVLT. **b**, GCaMP6m fluorescence in VP sensors before (baseline) and after application of blue light (50 ms, 22 mW, 5 Hz, 30 s) and after wash. **c**, Changes in fluorescence induced by blue light (mean ± s.e.m.; $^{****}P < 0.0001$, paired *t*-test). **d**, Firing rate (mean ± s.e.m.) of OVLT neurons recorded in slices with or without light and/or SR49059 expressed as percent of average firing rate of control cells during BP in ChETA mice (Kruskal–Wallis one-way ANOVA on ranks and Dunn's post-hoc test; $^{*}P < 0.05$; NS, $P > 0.05$) or during AP in ArchT mice (control vs. yellow light, Mann–Whitney test; other comparisons, Kruskal–Wallis one-way ANOVA; 2-s excerpts shown above bars). **e**, Number of c-Fos^{+} OVLT cells in wild-type and $V1aR^{-/-}$ mice (mean ± s.e.m.; two-way ANOVA and Holm Sidak post-hoc test). **f**, Changes in the rate of water intake expressed as percent of average values in BP in wild-type and $V1aR^{-/-}$ mice (mean ± s.e.m.; paired *t*-test). **g**, Water intake (5-min bins) in seven trials from six ChETA mice in which blue light was applied at ZT20.5 (30 min, 22 mW). Changes in water intake induced by blue or yellow light (ZT20.5–21) expressed as percent of average intake during corresponding baselines (ZT19.5–20.5; mean ± s.e.m.; $^{**}P < 0.01$; blue light, paired *t*-test; yellow light, Wilcoxon test). **h**, Water intake (5-min bins) in six trials from four ArchT mice in which yellow light was applied at ZT22.5 (30 min, 13 mW). Changes in water intake induced by yellow or blue light (ZT22.5–23) expressed as a percent of average intake during corresponding baselines (ZT21.5–22.5; mean ± s.e.m.; paired *t*-test). *n* as indicated.

the AP (Fig. 4h), indicating that VP released from the axon terminals of SCN neurons is necessary to drive anticipatory thirst.

Our study reveals that increased water intake during the AP is not motivated by physiological need, but anticipates and protects against overnight dehydration. How the central clock mediates adaptive behaviours of this kind was heretofore unknown. Our findings indicate that activity-dependent VP release from the axon terminals of clock neurons onto OVLT neurons is necessary and sufficient to generate anticipatory thirst. Whether the SCN drives other behaviours by VP neurotransmission remains to be determined.

Online Content Methods, along with any additional Extended Data display items and Source Data, are available in the online version of the paper; references unique to these sections appear only in the online paper.

Received 31 March; accepted 15 August 2016.

1. Mills, J. N. Human circadian rhythms. *Physiol. Rev.* **46,** 128–171 (1966).
2. Mohawk, J. A., Green, C. B. & Takahashi, J. S. Central and peripheral circadian clocks in mammals. *Annu. Rev. Neurosci.* **35,** 445–462 (2012).
3. Hastings, M. H., Maywood, E. S. & O'Neill, J. S. Cellular circadian pacemaking and the role of cytosolic rhythms. *Curr. Biol.* **18,** R805–R815 (2008).
4. Antle, M. C. & Silver, R. Orchestrating time: arrangements of the brain circadian clock. *Trends Neurosci.* **28,** 145–151 (2005).
5. Johnson, R. F., Beltz, T. G., Thunhorst, R. L. & Johnson, A. K. Investigations on the physiological controls of water and saline intake in C57BL/6 mice. *Am. J. Physiol. Regul. Integr. Comp. Physiol.* **285,** R394–R403 (2003).
6. Spiteri, N. J. Circadian patterning of feeding, drinking and activity during diurnal food access in rats. *Physiol. Behav.* **28,** 139–147 (1982).
7. Bourque, C. W. Central mechanisms of osmosensation and systemic osmoregulation. *Nat. Rev. Neurosci.* **9,** 519–531 (2008).
8. Barney, C. C. & Folkerts, M. M. Thermal dehydration-induced thirst in rats: role of body temperature. *Am. J. Physiol.* **269,** R557–R564 (1995).
9. Fitzsimons, J. T. Angiotensin, thirst, and sodium appetite. *Physiol. Rev.* **78,** 583–686 (1998).
10. Johnson, A. K. & Buggy, J. Periventricular preoptic-hypothalamus is vital for thirst and normal water economy. *Am. J. Physiol.* **234,** R122–R129 (1978).
11. McKinley, M. J., Denton, D. A. & Weisinger, R. S. Sensors for antidiuresis and thirst—osmoreceptors or CSF sodium detectors? *Brain Res.* **141,** 89–103 (1978).
12. Ramsay, D. J., Thrasher, T. N. & Keil, L. C. The organum vasculosum laminae terminalis: a critical area for osmoreception. *Prog. Brain Res.* **60,** 91–98 (1983).
13. McKinley, M. J., Denton, D. A., Oldfield, B. J., De Oliveira, L. B. & Mathai, M. L. Water intake and the neural correlates of the consciousness of thirst. *Semin. Nephrol.* **26,** 249–257 (2006).
14. Farrell, M. J. *et al.* Cortical activation and lamina terminalis functional connectivity during thirst and drinking in humans. *Am. J. Physiol. Regul. Integr. Comp. Physiol.* **301,** R623–R631 (2011).
15. Hollis, J. H., McKinley, M. J., D'Souza, M., Kampe, J. & Oldfield, B. J. The trajectory of sensory pathways from the lamina terminalis to the insular and cingulate cortex: a neuroanatomical framework for the generation of thirst. *Am. J. Physiol. Regul. Integr. Comp. Physiol.* **294,** R1390–R1401 (2008).
16. Stephan, F. K. Circadian rhythms in the rat: constant darkness, entrainment to T cycles and to skeleton photoperiods. *Physiol. Behav.* **30,** 451–462 (1983).
17. Satinoff, E. & Prosser, R. A. Suprachiasmatic nuclear lesions eliminate circadian rhythms of drinking and activity, but not of body temperature, in male rats. *J. Biol. Rhythms* **3,** 1–22 (1988).
18. Kalsbeek, A. *et al.* SCN outputs and the hypothalamic balance of life. *J. Biol. Rhythms* **21,** 458–469 (2006).
19. Moore, R. Y., Speh, J. C. & Leak, R. K. Suprachiasmatic nucleus organization. *Cell Tissue Res.* **309,** 89–98 (2002).
20. Abrahamson, E. E. & Moore, R. Y. Suprachiasmatic nucleus in the mouse: retinal innervation, intrinsic organization and efferent projections. *Brain Res.* **916,** 172–191 (2001).
21. Buijs, R. M. & Kalsbeek, A. Hypothalamic integration of central and peripheral clocks. *Nat. Rev. Neurosci.* **2,** 521–526 (2001).
22. Chen, T. W. *et al.* Ultrasensitive fluorescent proteins for imaging neuronal activity. *Nature* **499,** 295–300 (2013).
23. Serradeil-Le Gal, C. *et al.* Nonpeptide vasopressin receptor antagonists: development of selective and orally active V1a, V2 and V1b receptor ligands. *Prog. Brain Res.* **139,** 197–210 (2002).
24. Gunaydin, L. A. *et al.* Ultrafast optogenetic control. *Nat. Neurosci.* **13,** 387–392 (2010).
25. Han, X. *et al.* A high-light sensitivity optical neural silencer: development and application to optogenetic control of non-human primate cortex. *Front. Syst. Neurosci.* **5,** 18 (2011).
26. Serradeil-Le Gal, C. *et al.* An overview of SSR149415, a selective nonpeptide vasopressin V(1b) receptor antagonist for the treatment of stress-related disorders. *CNS Drug Rev.* **11,** 53–68 (2005).

Acknowledgements This work was supported by a Foundation Grant from the Canadian Institutes of Health Research (FDN 143337), a James McGill Chair, and a Studentship awarded by the Research Institute of the McGill University Health Centre (RIMUHC). The RIMUHC receives generous funding from the Fonds de Recherche Québec Santé. We thank M. Bouvier for human V1aR; H. Gainer for anti-VP neurophysin primary antibodies; and N. Cermakian, K-F. Storch, and M. Prager-Khoutorsky for comments on an early draft of the manuscript.

Author Contributions C.G. and C.W.B. designed the study, interpreted the results, and wrote the manuscript. C.Z. contributed to experiments involving HEK cells and single-cell RT–PCR. C.G. performed all other experiments.

Author Information Reprints and permissions information is available at www.nature.com/reprints. The authors declare no competing financial interests. Readers are welcome to comment on the online version of the paper. Correspondence and requests for materials should be addressed to C.W.B. (charles.bourque@mcgill.ca).

Reviewer Information *Nature* thanks C. Colwell, H. de la Iglesia, H. Okamura and the other anonymous reviewer(s) for their contribution to the peer review of this work.

METHODS

Animals. Animals were treated in strict accordance with the guidelines outlined by the Canadian Council on Animal Care (http://www.ccac.ca/), and experiments adhered to protocols approved by the Facility Animal Care Committee of McGill University (protocol no. 1190). Long–Evans rats (80−150 g) and C57/B6 mice (60−90 d) were obtained from Charles River Laboratories. VP-Cre (VP-IRES2-Cre-D) knock-in mice were bred in our colony with either ChETA (R26-CAG-LSL-2XChETA-tdTomato) or ArchT mice (Ai40D; obtained from Jackson Laboratories). V1aR knock-out ($V1aR^{-/-}$) mice were bred in our colony (obtained from J. N. Crawley)[27]. All experiments were performed on male animals, except for one experiment (Extended Data Fig. 8) where a female was used. *In vitro* experiments were performed on mice aged 2−4 months, experiments on rats were done on animals weighing 80−150 g, and *in vivo* mouse experiments were done on animals aged 2−3 months. Animals were subjected to a strict 12 h:12 h light:dark cycle.

Water-intake monitoring. C57/B6 mice were individually housed in computer-interfaced metabolic Oxylet cages from PanLab (Harvard Apparatus) to measure water intake. Animals were placed in cages and allowed to habituate to the cages for 4−6 days. To obtain the average circadian profile of water intake, we obtained hourly averages from each subject between ZT6.5 and ZT6.5 on the following day. Data files were analysed using Metabolism (version 2.1.04; PanLab) and Microsoft Excel. Statistical analysis was performed in Sigmaplot (Version 12.3, Systat Software).

Physiological parameters. Since we cannot obtain serial measures of serum osmolality in individual C57/B6 mice, we used a group approach whereby data were collected from multiple (3−18) subjects that were killed at each time point tested. To this end, mice were anaesthetized with isoflurane and rapidly decapitated to obtain blood samples, core body temperature using a digital thermometer, and haematocrit using a ZipCombo Centrifuge from LW Scientific. Blood samples were placed on ice and allowed to clot at 2−4 C for 60 min, after which they were centrifuged for 5 min, and serum osmolality was measured in duplicate using a micro-osmometer (Advanced Instruments).

Water restriction. The objective of this experiment (Fig. 1c, d), was to deny the surge in water intake, while preserving water intake levels during the AP equivalent to levels during the BP. Because water intake between ZT21.5 and ZT22.5 is equivalent to water intake between ZT19.5 and ZT21.5 (BP), we allowed water intake to proceed until ZT22.5 before removing access to water. Water was removed from C57/B6 mouse cages at either ZT22.5 (no AP surge allowed) or ZT23.5 (AP surge allowed). Access to water overnight was denied to prevent compensatory drinking and allow a specific evaluation of the impact of the AP surge alone. Animals were then killed at ZT10 and blood samples were collected to measure serum osmolality and haematocrit as explained above.

OVLT firing rate. Horizontal hypothalamic slices containing the OVLT and SCN were prepared from 2−4-month-old male ArchT or ChETA mice. These animals were not subjected to any behavioural or optogenetic experiments before slice preparation. Mice anaesthetized with isoflurane were killed by decapitation at ZT18–18.5. The brain was rapidly removed and immersed in near-freezing (0–4 °C) oxygenated (95% O_2, 5% CO_2) artificial mouse cerebrospinal fluid (AMCSF) composed of the following (in mM): 128 NaCl, 3 KCl, 1.23 NaH_2PO_4, 1.48 $MgCl_2$, 2 $CaCl_2$, 25.95 $NaHCO_3$ and 10 D-glucose (all obtained from Sigma except for NaCl and $CaCl_2$, which were purchased from Fisher Scientific). A trimmed block of brain was glued, cortex down with the rostral pole facing upwards, to a mounting block angled at 34° relative to the horizontal plane. A single 350-μm slice was then obtained (Extended Data Fig. 2) and transferred dorsal side up to a beaker containing warmed (32 °C) oxygenated AMCSF and allowed to incubate for 60 min. The slice was then transferred dorsal side up to a recording chamber where it was perfused with warmed (32 °C) oxygenated AMCSF at a rate of 2–3 ml min^{-1}. Cells were observed on a black and white monitor using an Olympus BX51WI upright microscope coupled to a video camera. Electrodes were visually guided to the cell using a motorized micromanipulator (s.d. Instruments) and cell-attached recordings were made using a MultiClamp 700B amplifier (Molecular Devices). Membrane voltage was digitized via a Digidata 1440A interface coupled to a personal computer running Clampex 10.3 software (Molecular Devices). A band-pass filter was applied during cell-attached recordings (800 Hz–1.8 kHz). Patch pipettes were back-filled with AMCSF and their resistance in the bath was 5.5−7.5 MΩ. Cell-attached recordings for firing rates of OVLT neurons during the BP were performed from ZT19.5 to ZT21.5 and during the AP from ZT21.5 to ZT23.5. Cell-attached recordings from OVLT neurons were obtained by making a loose seal. If cells did not fire during the recording, a brief zap of 25 μs was delivered at the end of the recording to evoke firing in order to confirm they were indeed silent cells that were otherwise capable of firing detectable action potentials. The average firing rate was calculated by dividing the total number of spikes recorded by the duration of the recording period (60 s). One cell was excluded from this analysis because its firing rate was more than four times greater than the standard deviation of the group.

Evans blue injection. Evans blue was used to evaluate the boundaries of the OVLT in mice as previously reported for rat[28]. Briefly, mice were anaesthetized with isoflurane and injected intravenously with 0.2 ml of 1% Evans blue dissolved in PBS. After 15 min, the animals were transcardially perfused with 20 ml PBS, and then the brain was extracted and fixed by immersion for at least 48 h in 4% paraformaldehyde (PFA) dissolved in PBS. Serial sections (50 μm thick) were cut and mounted onto slides, and Evans blue fluorescence was visualized using RS Image (version 1.9.2; Roper Scientific) using a 10× objective (na = 0.4) attached to an Olympus BX51WI upright microscope and a CoolSnap HQ_2 camera (Photometrics). Fluorescence was observed at 700 nm and excited at 650 nm using an X-Cite XLED1 system (Lumen Dynamics, Excelitas Canada) and a BrightLine Pinkel filter set (DA/FI/TR/Cy5-4X-B-OMF; Semrock).

Retrograde fluorescent microspheres. C57/B6 mice (60 d) were anaesthetized with isoflurane and stereotaxically injected with FluoSpheres (0.04 μm, yellow-green fluorescent 488 nm, 5% solids, azide free; ThermoFisher Scientific) into the OVLT (100−200 nl; from Bregma with a 7° vertical angle, X: 1.2 mm, Y: 0 mm, Z: −4.6 or −4.7; Extended Data Fig. 3) with a Neuros syringe (0.5 μl, 32 gauge, Hamilton) over 5−10 min. The spheres were allowed to be retrogradely transported for 7 days, after which the animals were anaesthetized with isoflurane and perfused via the heart with 10 ml PBS followed by 300 ml PBS containing 4% PFA. The brains were extracted and postfixed by immersion for 48 h in 4% PFA in PBS. A vibratome was used to obtain serial coronal tissue sections (50 μm thick). Sections were blocked with 10% normal goat serum (in PBS containing 0.3% Triton-X100) and incubated overnight at 4 °C with primary antibodies. Following wash, sections were incubated for 1 h with fluorescently labelled secondary antibodies. Sections were then washed and mounted on coverslips using Prolong Gold Antifade reagent (Life Technologies). All images were acquired using a confocal microscope (FV1000, Olympus Canada). The following primary antibodies were used: PS41 anti-VP neurophysin mouse monoclonal antibody (1:50), and VA4 anti-VP neurophysin rabbit polyclonal antibody (1:1000) developed and contributed by H. Gainer (National Institutes of Health, Bethesda, MD). Secondary antibodies were fluorescently labelled Alexa Fluor-conjugated (568 nm and 647 nm; Life Technologies; 1:500).

c-Fos analysis. Brains were extracted from wild-type and $V1aR^{-/-}$ mice at ZT21.5–22 (for BP analysis) and ZT23.5–24 (for AP analysis) and immersion fixed in 4% PFA. Tissue sections (50 μm thick) from wild-type and $V1aR^{-/-}$ mice were processed using a rabbit polyclonal c-Fos antibody (EMD Millipore; 1:5,000) with a chicken anti-NeuN (Hexaribonucleotide Binding Protein-3a) polyclonal antibody (ABN91, 1:500; EMD Millipore; in OVLT), or with PS41 (as above) in the SCN. Secondary antibodies were fluorescently labelled Alexa Fluor-conjugated (488 nm, 568 nm, and 647 nm; Life Technologies; 1:500). Cells were considered c-Fos-positive if they were >100% above background. For OVLT analysis, cells were counted in a 200 × 200 μm field centred over the nucleus. For SCN, density was assessed over the entire nucleus. Sample size (n) refers to the number of sections analysed, which were obtained from 2 animals in each group.

SCN firing rate. Coronal 300-μm slices were obtained from mouse brain as described above. These animals were not subjected to any behavioural or optogenetic experiments before slice preparation. Cell-attached recordings were obtained from visually identified fluorescent VP cells (see Extended Data Fig. 4). Green fluorescence in ArchT mice was detected using EN GFP 41017 filter cube (Chroma Technology) and red fluorescence in ChETA mice was detected using 49004 (Chroma Technology). Firing rate was assessed as described above. One cell was excluded from this analysis because its firing rate was more than four times greater than the standard deviation of the group.

Rat hypothalamic slices. Horizontal hypothalamic slices were obtained from male rats as previously described[29]. Briefly, rats were killed by decapitation using a small rodent guillotine. The brain was rapidly removed and immersed in near-freezing (0–4 °C) oxygenated (95% O_2, 5% CO_2) artificial rat cerebrospinal fluid (ARCSF) composed of the following (in mM) 120 NaCl, 3 KCl, 1.23 NaH_2PO_4, 1.48 $MgCl_2$, 2 $CaCl_2$, 25.95 $NaHCO_3$ and 10 D-glucose. A trimmed block of brain was glued cortex-down with the rostral pole facing upwards to a mounting block angled at 38° relative to the horizontal plane. The assembly was then placed in a vibratome and a first cut was made to discard the tissue lying anterior and ventral to the optic tracts and most of the optic chiasma. A single 400-μm slice was then obtained and transferred dorsal side up to a beaker containing warmed (32 °C) oxygenated ARCSF and allowed to rest for 60 min. Slices were then placed in a warmed (32 °C) recording chamber perfused at a rate of 2–3 ml min^{-1}.

VP detection with HEK293 biosensors in rat brain slices. HEK293 cells (gift from Sal Carbonetto; not tested for mycoplasma) were kept in DMEM (Wysent) at 37 °C and 5% CO_2. The co-transfection of pGP-CMV-avp 6m (AddGene) and the human V1aR (provided by M. Bouvier, University of Montreal, QC) (2.5 μg each) was done using Lipofectamine 3000 (Invitrogen). 24 to 48 h after transfection the cultures were treated with trypsin and cells were lifted and plated over recently cut rat horizontal brain slices resting in beakers as explained above. Preparations were allowed to rest for 2 h, allowing cells to attach to the slice before starting the experiment. Experiments were completed during the subjective BP (ZT19.5−21.5) when VP release was low. Slices were carefully placed in the recording chamber, and a bipolar electrical stimulating electrode (pair of 65 μm o.d. platinum wires) was placed in the SCN. Electrical pulses (20–80 μA, 0.1−0.5 ms; 10 Hz, 40 s) were delivered via an isolated stimulator (DS2, Digitimer) triggered via a programmable digital timer (D4030, Digitimer). Fluorescence of GCaMP6m in HEK293 cells was observed using the EN GFP 41017 filter cube. Images were collected using Imaging Workbench 6.0 (INDEC BioSystems) at a rate of 1 image every 5 s (exposure 0.2 s). In control conditions, only pGP-CMV-GCaMP6m was transfected and not V1aR. Dose–response analysis and specificity were assessed on HEK293 cells plated on glass coverslips (Extended Data Fig. 5). VP dissolved in water (0.1 mM) was kept frozen until required. All images were analysed using Fiji[30]. Fluorescence in regions of interests (HEK cells) was corrected for bleaching determined by fitting a single exponential. Background fluorescence was subtracted from all values. Values of fluorescence at various time points were expressed relative to baseline. Changes in fluorescence relative to baseline (average of 30 s before stimulation) were determined from the average of values observed during a 30-s period following the onset of the response.

Electrophysiological analysis of rat-brain slices. Slices were obtained as mentioned above. Bicuculline was dissolved directly into the ARCSF at the required concentration (10 μM). Kynurenate was first dissolved into a small volume (<0.5 ml) of 1 N NaOH and subsequently diluted into a larger volume of ARCSF at the required concentration (3 mM). All whole-cell experiments were performed in the presence of kynurenate and bicuculline. All recordings were made during subjective night (ZT5−11). Whole-cell recordings from OVLT neurons were made using patch pipettes prepared from glass capillary tubes (1.2-mm outer diameter, A-M Systems) filled with the appropriate internal solution. Pipette resistance in the bath was 3.5−5.5 MΩ. Series resistance was 10−30 MΩ. A bipolar stimulating electrode was placed in the SCN at the beginning of each recording session. Electrical pulses (20–80 μA, 0.1−0.5 ms; 10Hz, 30 s) were delivered as described above. For gap-free whole-cell current clamp recordings, pipettes were back-filled with a solution containing the following (in mM): 140 K^+-gluconate, 2 $MgCl_2$, 10 HEPES, 2 ATP(Na_2), 0.4 GTP(Na_2) (pH adjusted to 7.25 with NaOH). Baseline average firing rates were calculated over a window of 60 s immediately preceding SCN stimulation, and the corresponding voltage was obtained from the peak of an all-points voltage histogram. SCN stimulation evoked firing rates were calculated over a window of 60 s during the maximal firing response within 2 min of the end of stimulation. Post-stimulation voltage was obtained during the corresponding period. Current clamp analysis (Fig. 3f) was restricted to cells maintained by current injection between −35 and −50 mV (values not corrected for liquid junction). Aliquots of SR49059 dissolved in DMSO (10 mM) were diluted into ARCSF to achieve a final concentration of 10 μM. For whole-cell voltage clamp experiments, steady state current–voltage ($I-V$) relations were obtained from the current responses induced by slow voltage ramps (−110 to +10 mV; 2 s, V_h −50mV). Pipettes were backfilled with solutions corresponding to the experiment in question. K^+ internal solutions were composed of the following (in mM): 140 K^+-gluconate, 2 $MgCl_2$, 10 HEPES, 2 ATP(Na_2), 0.4 GTP(Na_2) and 5 QX314-Br (pH adjusted to 7.25 with NaOH). Cs^+ internal solutions were composed of the following (in mM): 140 CsMeS, 10 HEPES, 2 $MgCl_2$, 2 ATP(Na_2), 0.4 GTP(Na_2) and 5 QX314-Br (pH adjusted to 7.25 with NaOH). Cl^- internal solutions were composed of the following (in mM): 100 CsMeS, 40 CsCl, 10 HEPES, 2 $MgCl_2$, 2 ATP(Na_2), 0.4 GTP(Na_2) and 5 QX314-Br (pH adjusted to 7.25 with NaOH). Currents induced in OVLT neurons induced by SCN stimulation were evaluated as the difference current obtained by subtracting the average of two $I-V$ curves taken 1 min after SCN stimulation from the average of two $I-V$ curves recorded preceding SCN stimulation. When required, a lowpass filter was applied to the difference current trace (lowpass 80−200 Hz). SCN-induced changes in membrane conductance were quantified as the slope of the difference current $I-V$ curve, measured over a range of 20 mV below the reversal potential. In the analysis of Fig. 3i, j, two cells were excluded because SCN-induced currents did not show a reversal potential.

VP detection using biosensors in mouse-brain slices. VP release caused by light-induced depolarization of SCN VP axons was performed using co-transfected HEK293 cells prepared as described above, in horizontal slices prepared from ChETA mice. Blue light (473 nm DPSS Laser system, Laserglow Technologies) was delivered over the OVLT (50 ms, 22 mW, 5 Hz) for 30 s through a fibre-optic probe (slim titanium magnetic receptacle, 200 μm fibre optic diameter/240 μm diameter with coating/5.5 mm length numerical aperture 0.22, Doric Lenses), connected to a mono fibre-optic patchcord (2 m) via a fibre-optic rotary joint.

Optogenetic manipulation of OVLT neuron firing. Horizontal slices were prepared from either ChETA or ArchT mice. Cell-attached recordings were performed as previously described. Blue light was delivered over the OVLT as previously described (50 ms, 22 mW, 5 Hz) for 30−60 s in ChETA slices during the BP (ZT19.5−21.5). Additional light intensities were used to determine threshold sensitivity (Extended Data Fig. 9). Yellow light (589 nm, 13 mW, constant light, DPSS laser system, Laserglow Technologies) was delivered over the OVLT in ArchT slices during the AP (ZT21.5−23.5). SR49059 (10 μm) was bath-applied during experiments as noted. Firing rates were calculated by counting the number of spikes during 30−60 s. Firing rates were normalized to the average baseline firing of the time period in question.

Optogenetic manipulation of SCN neuron firing. Coronal slices were prepared from ChETA or ArchT male or female mouse brains. Cell-attached recordings were performed on identified VP neurons as previously described. Once sufficient baseline was recorded (2–3 min), blue light (for ChETA) or yellow light (for ArchT) was delivered to the slice. Analysis of light-induced changes in firing rate was performed by comparing firing rates averaged during 30−60 s periods recorded before and during light stimulation.

***In vivo* optogenetics.** ChETA and ArchT male mice (60–90 d) were stereotaxically implanted with a slim magnetic receptacle fibre-optic cannulas (5.5 mm, Doric Lenses) above the OVLT (from bregma with a 7° vertical angle, X: 1.18 mm, Y: 0 mm, Z: –4.5; ref. 31). Cannulas were initially glued to the brain using Metabond (C&B Metabond, Parkell), allowed to dry, then covered with a generous coat of dental cement (Stoelting). Animals recovered for 7 days, after which they were handled for one week to allow habituation to handling and to the fibre-optic patchcord. For testing, animals were placed in metabolic cages on Thursday afternoons. On Mondays, the animals were trained by being connected to the patchcord during the appropriate test period (2.5 h), 1 h post-handling rest, 1 h baseline, 30 min test. Testing started on the following Tuesday. ChETA mice were tested from ZT18.5 to ZT21, and ArchT mice were tested from ZT20.5 to ZT23. During the test period they received either blue light (22 mW continuous or 50 ms, 22 mW, 5 Hz), or yellow light (13 mW continuous) on separate days. Water intake analysis was performed as described above. Following the last day of testing, animals were anaesthetized and decapitated. Optical implants were removed and brains were fixed by immersion for at least 48 h in 4% PFA dissolved in PBS. Serial coronal sections (50 μm thick) were cut to determine the position of the tip of the fibre-optic cannula. Experiments were rejected if the fibre-optic tip terminated rostral or caudal to the OVLT, or more than 200 μm dorsal from the dorsal surface of the OVLT.

Characterization of transgene expression in VP neurons. Serial coronal sections (50 μm thick) were cut from an ArchT mouse brain to analyse the expression of GFP in VP neurons. Sections were processed for immunohistochemistry as described above. A chicken anti-GFP primary antibody (1:1,000, AB13970, Abcam) was used to enhance detection of the fluorescence reporter and the PS41 mouse monoclonal anti-VP neurophysin antibody (1:50; H. Gainer, NIH[32,33]) was used to detect VP. Secondary antibodies were fluorescently labelled Alexa Fluor-conjugated (568 nm, and 647 nm; Life Technologies; 1:500). Images were analysed using ImageJ 1.50a (NIH) to count the number of VP-labelled SCN neurons and anti-GFP-labelled SCN neurons.

Single cell RT–PCR. As previously described[34], single OVLT neurons were aspirated from the slice using large autoclaved micropipettes (1−2 MΩ), which were backfilled with 1.5 μl of a solution containing RNaseIN (10 U μl^{-1}; Life Technologies). Upon contact and gigaseal formation, cells that fired action potentials (neurons) were sucked by negative pressure to collect cytoplasm, then lifted and completely suctioned into the electrode. The contents were then expelled by positive pressure into a 250-μl microcentrifuge tube containing 0.5 μl DNase I (1 U μl^{-1}; Fisher Scientific) and 1 × $MgCl_2$ buffer and stored over dry ice. Tubes were incubated at 37 °C for 30 min, and the reaction was stopped by adding 1 μl EDTA (25 mM) and incubated at 65 °C for 10 min. The RT reaction was then performed by adding 1 μl 50 μM Random Hexamer primers (Life Technologies), 0.25 μl RNaseIN (10 U μl^{-1}), 1 μl 0.1M DTT, 1 μl 50 mM MgCl2, 1 μl 10 mM (each) dNTPs mix (QIAGEN), 2 μl 5 × First Strand Buffer, and 0.25 μl SuperscriptIII (200 U μl^{-1}; ThermoFisher). The mix was incubated at 50 °C for 2 h and then the cDNA was stored at −20 °C. Nested PCR and nested multiplex single-cell PCR were performed using the following primers: Avpr1a ForOUT3 5′ATCCCATCCAAAACCACTCTGAGCG3′;

Avpr1a RevOUT3 5′GGTAACACTTGGAAGAAGGCGACCG3′; Avpr1a ForIN3 5′GAAGAGAGCGAGGTAAGGAAGGACGG3′; Avpr1a RevIN3 5′TGCGGGATGTCTTGCGTGGC3′; V1v ForOUT 5′ATGTGGTAGACATGAGGGAGCTAGAGGC3′; V1v RevOUT 5′AATCTTCCCACTGCTGGCAGCC3′; V1v ForIN 5′TCCAGGGACTAGCCTCATTGGTGGG3′; V1v RevIN 5′TGAGTTCTTCTAGCTTCAGTGTGGGGTG3′.

PCR amplicons were analysed on 2.5% agarose.

Statistical analysis. All group data are reported or displayed as means ± s.e.m. and the exact sample size is provided for each experimental group or condition either in the text or as indicated within or below bar graphs. Information about sample collection is also provided where relevant (for example, number of trials per animals, or sections per brain). Differences between groups (two-sided) were compared using Sigmaplot 12.0 (Systat Software). The software first assessed normality of the data distribution. In all cases where the normality test failed, a suitable non-parametric test was performed. All tests used for comparisons are specified in the text. No statistical methods were used to predetermine sample size. The experiments were not randomized. The investigators were not blinded to allocation during experiments and outcome assessment.

27. Hu, S. B. *et al.* Vasopressin receptor 1a-mediated negative regulation of B cell receptor signaling. *J. Neuroimmunol.* **135,** 72–81 (2003).
28. Prager-Khoutorsky, M. & Bourque, C. W. Anatomical organization of the rat organum vasculosum laminae terminalis. *Am. J. Physiol. Regul. Integr. Comp. Physiol.* **309,** R324–R337 (2015).
29. Trudel, E. & Bourque, C. W. A rat brain slice preserving synaptic connections between neurons of the suprachiasmatic nucleus, organum vasculosum lamina terminalis and supraoptic nucleus. *J. Neurosci. Methods* **128,** 67–77 (2003).
30. Schindelin, J. *et al.* Fiji: an open-source platform for biological-image analysis. *Nat. Methods* **9,** 676–682 (2012).
31. Franklin, K. B. & Paxinos, G. *The Mouse Brain in Stereotaxic Coordinates.* Third edn (Elsevier, 2008).
32. Altstein, M. & Gainer, H. Differential biosynthesis and posttranslational processing of vasopressin and oxytocin in rat brain during embryonic and postnatal development. *J. Neurosci.* **8,** 3967–3977 (1988).
33. Alstein, M., Whitnall, M. H., House, S., Key, S. & Gainer, H. An immunochemical analysis of oxytocin and vasopressin prohormone processing in vivo. *Peptides* **9,** 87–105 (1988).
34. Zaelzer, C. *et al.*. ΔN-TRPV1: A molecular co-detector of body temperature and osmotic stress. *Cell Reports* **13,** 23–30 (2015).

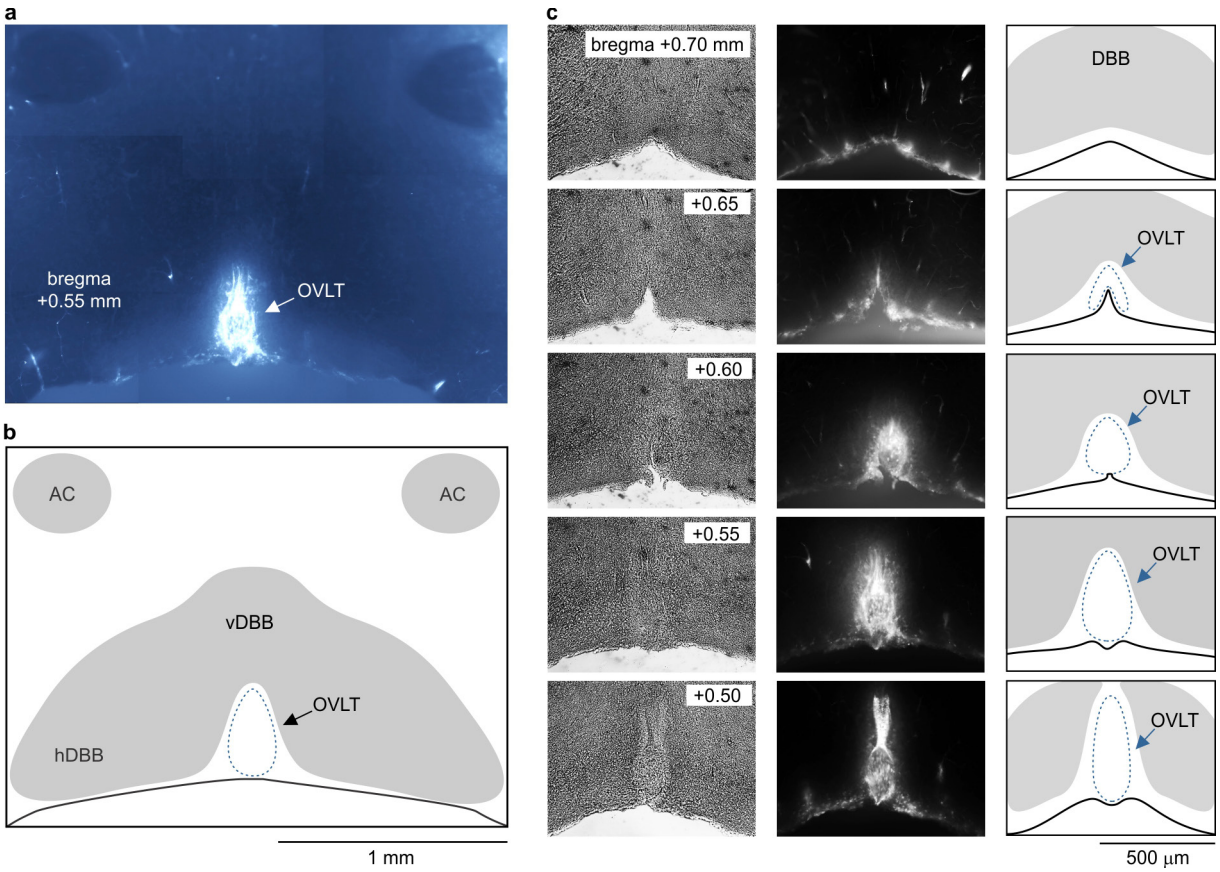

Extended Data Figure 1 | Anatomical outline of the mouse OVLT determined with Evans blue. a, Micrograph shows fluorescence (excitation 650 nm, emission 700 nm) in a 50-µm-thick coronal section taken through the anterior hypothalamus of a mouse injected intravenously with 1% Evans blue. The section corresponds to a plane lying 0.55 mm rostral to the bregma as defined elsewhere[31]. **b**, Schematic illustrating the outline of the OVLT and surrounding structures including the anterior commissure (AC), ventral diagonal band of Broca (vDBB), and horizontal diagonal band of Broca (hDBB). Scale bar applies to **a** and **b**. **c**, Panels show brightfield images (left), Evans blue fluorescence (middle), and schematics (right) in consecutive coronal sections spanning the entire rostro-caudal extent of the OVLT. Position relative to bregma is indicated on brightfield panels.

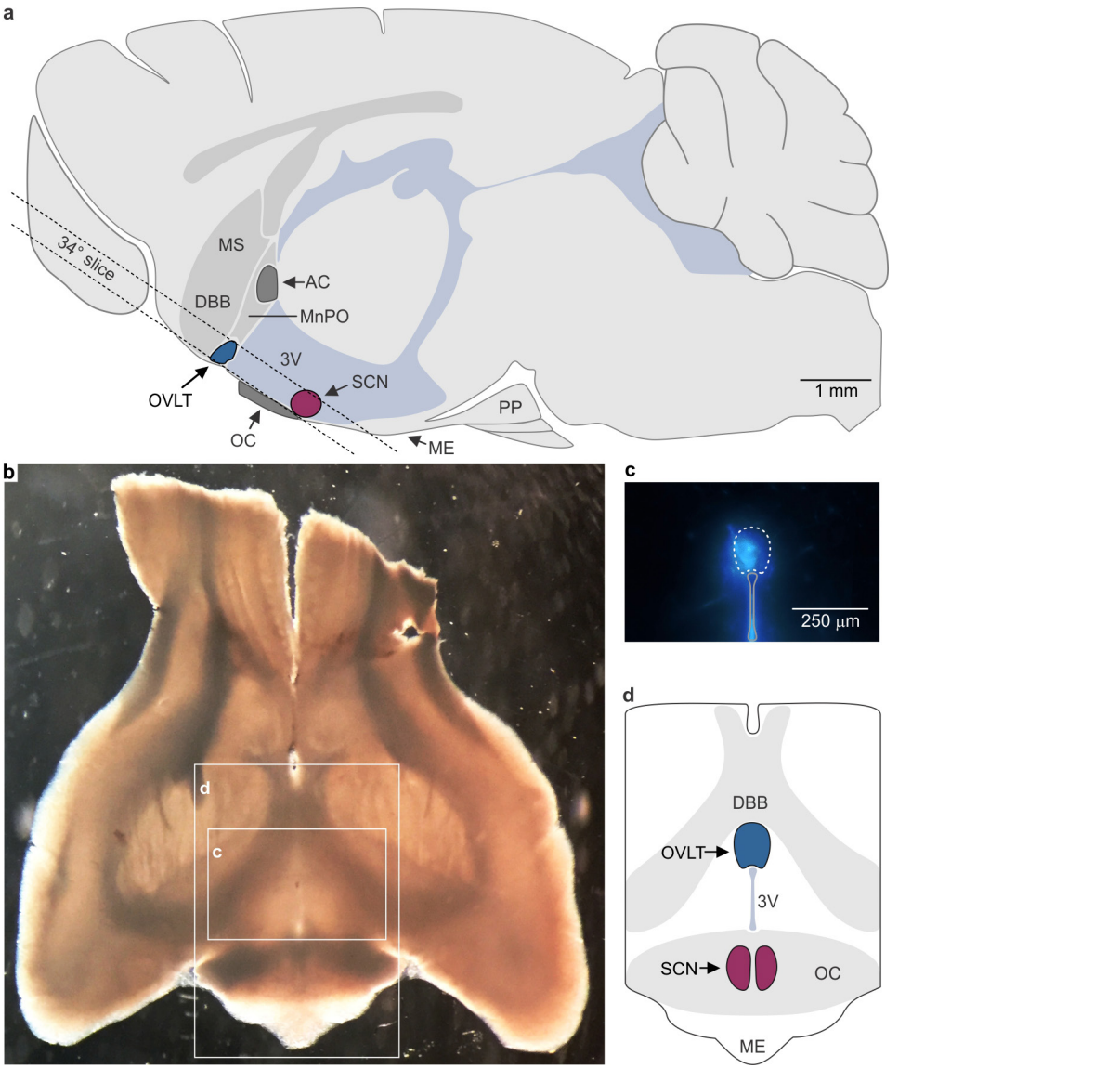

Extended Data Figure 2 | Preparation of angled slices of mouse hypothalamus that retain the OVLT and SCN. a, Schematic diagram showing the relative positions of the OVLT, SCN and other structures in the sagittal plane as defined elsewhere[31]. Median eminence (ME), median preoptic nucleus (MnPO), medial septum (MS), optic chiasma (OC), posterior pituitary (PP), third ventricle (3V). The brain slice was obtained at an angle of 34° relative to the horizontal plane. **b**, Brightfield image of a horizontal slice (plane as shown in **a**) obtained from a mouse injected intravenously with 1% Evan's blue. **c**, Evans blue fluorescence observed in the same slice in the small rectangular region identified in **b**. **d**, Schematic diagram illustrating various structures retained in the slice preparation (area shown by large rectangle in **b**).

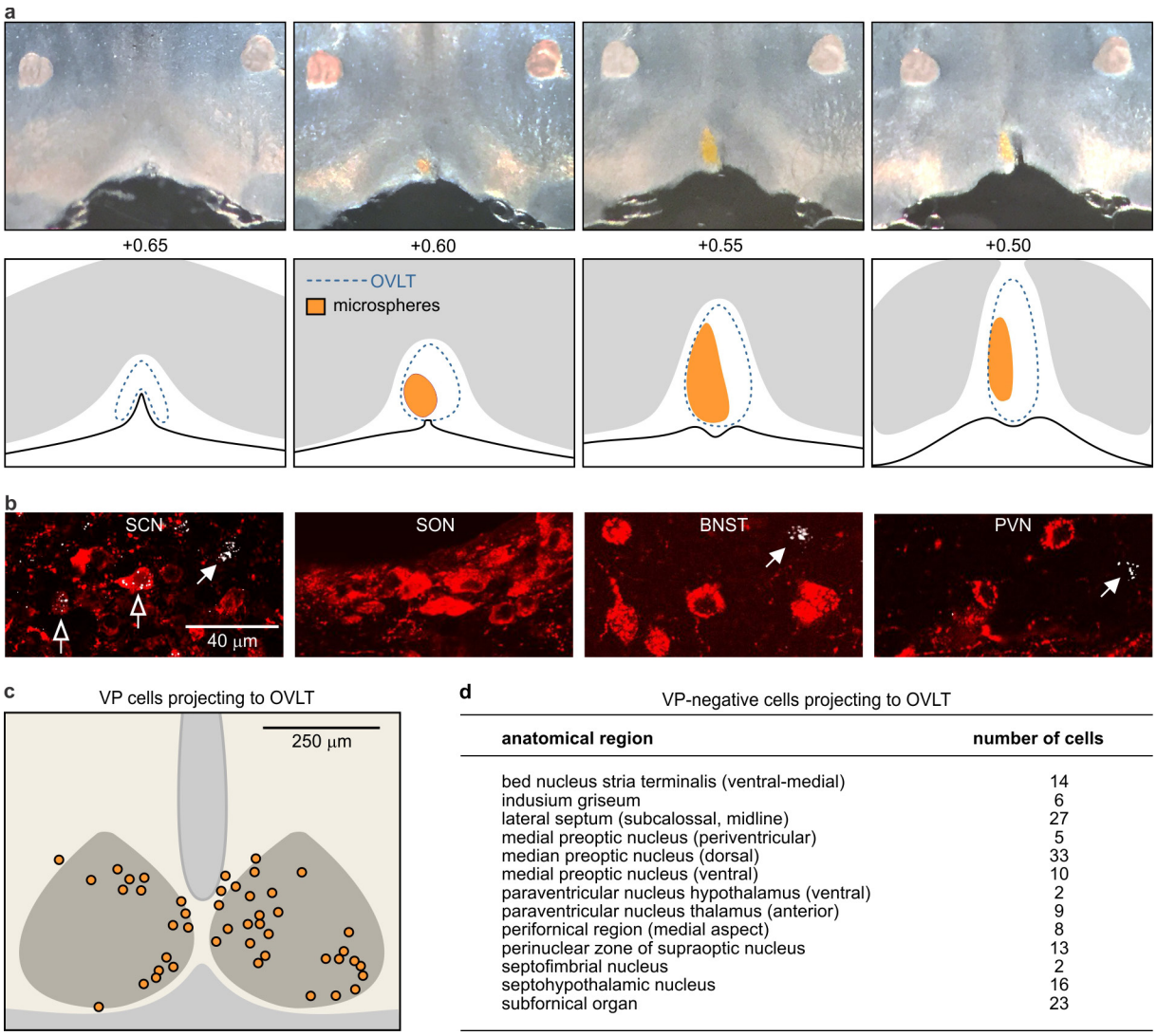

d

VP-negative cells projecting to OVLT

anatomical region	number of cells
bed nucleus stria terminalis (ventral-medial)	14
indusium griseum	6
lateral septum (subcalossal, midline)	27
medial preoptic nucleus (periventricular)	5
median preoptic nucleus (dorsal)	33
medial preoptic nucleus (ventral)	10
paraventricular nucleus hypothalamus (ventral)	2
paraventricular nucleus thalamus (anterior)	9
perifornical region (medial aspect)	8
perinuclear zone of supraoptic nucleus	13
septofimbrial nucleus	2
septohypothalamic nucleus	16
subfornical organ	23

Extended Data Figure 3 | Identification of SCN VP neurons projecting to the OVLT. a, Top, consecutive coronal bright-field micrographs showing the site of microsphere injection in one of three mice tested. Note the presence of material (orange) in three of the sections. Bottom, schematics illustrating the location of the microspheres (orange) within the area encompassing the OVLT. **b**, Representative sections from four brain areas containing VP-immunoreactive neurons (red) obtained from the brain shown in **a**: SCN, supraoptic nucleus (SON), bed nucleus of the stria terminalis (BNST) and the hypothalamic paraventricular nucleus (PVN). Note that only the SCN contains retrogradely labelled VP neurons (open arrows), whereas neurons containing retrogradely transported beads in BNST and PVN are VP-negative (arrows). **c**, Schematic diagram illustrating the positions of all 46 VP-positive neurons projecting to the OVLT for the brain shown in **a**. **d**, Table listing other brain areas containing neurons projecting to the OVLT for the brain shown in **a**. Only coronal sections positioned between +0.14 and −0.7 mm relative to Bregma were analysed (sites identified according to ref. 31).

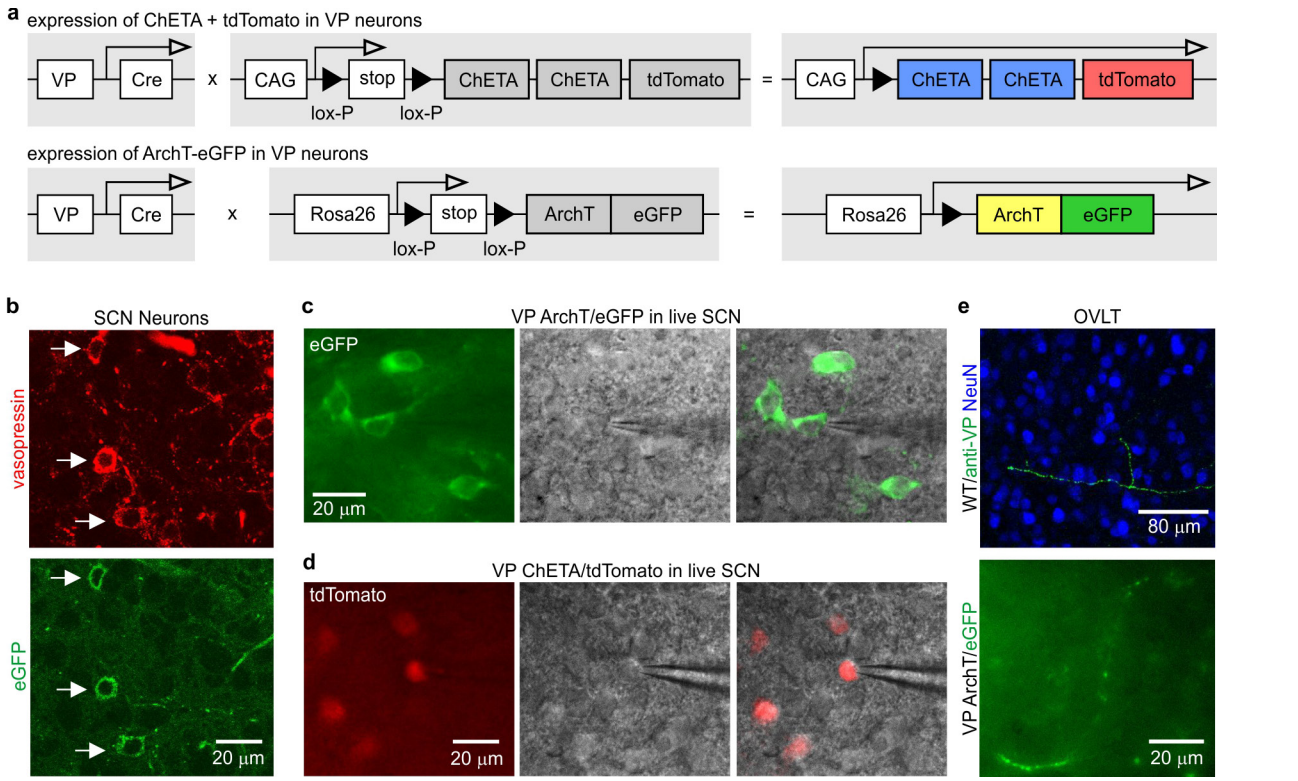

Extended Data Figure 4 | Transgenic mice expressing optogenetic probes and fluorescent reporters in VP neurons. a, Schematic illustrating the strategies used to produce mice in which VP neurons selectively express ChETA and tdTomato or ArchT and eGFP. **b**, Panels show the presence of VP (red, upper) and eGFP (green, lower) in an immunolabelled section through the SCN. Note that neurons containing eGFP are VP-positive (arrows), but that not all VP neurons contain eGFP. An analysis of five sections indicated that 41% of the VP SCN neurons (93/225 cells) expressed the fluorescent reporter. **c**, Left, live VP neurons identified by the presence of eGFP in the SCN of a hypothalamic slice prepared from an ArchT mouse. One cell is being targeted with a patch clamp micropipette. Middle, bright field; right, merge. **d**, Patch clamping of SCN VP neurons identified by the expression of tdTomato in ChETA mice (layout as in **c**). **e**, VP containing fibres are visible by immunolabelling in the wild-type OVLT (upper panel; VP in green, NeuN in blue), and by eGFP expression in the OVLT of ArchT mice (lower) or tdTomato expression in ChETA mice (not shown).

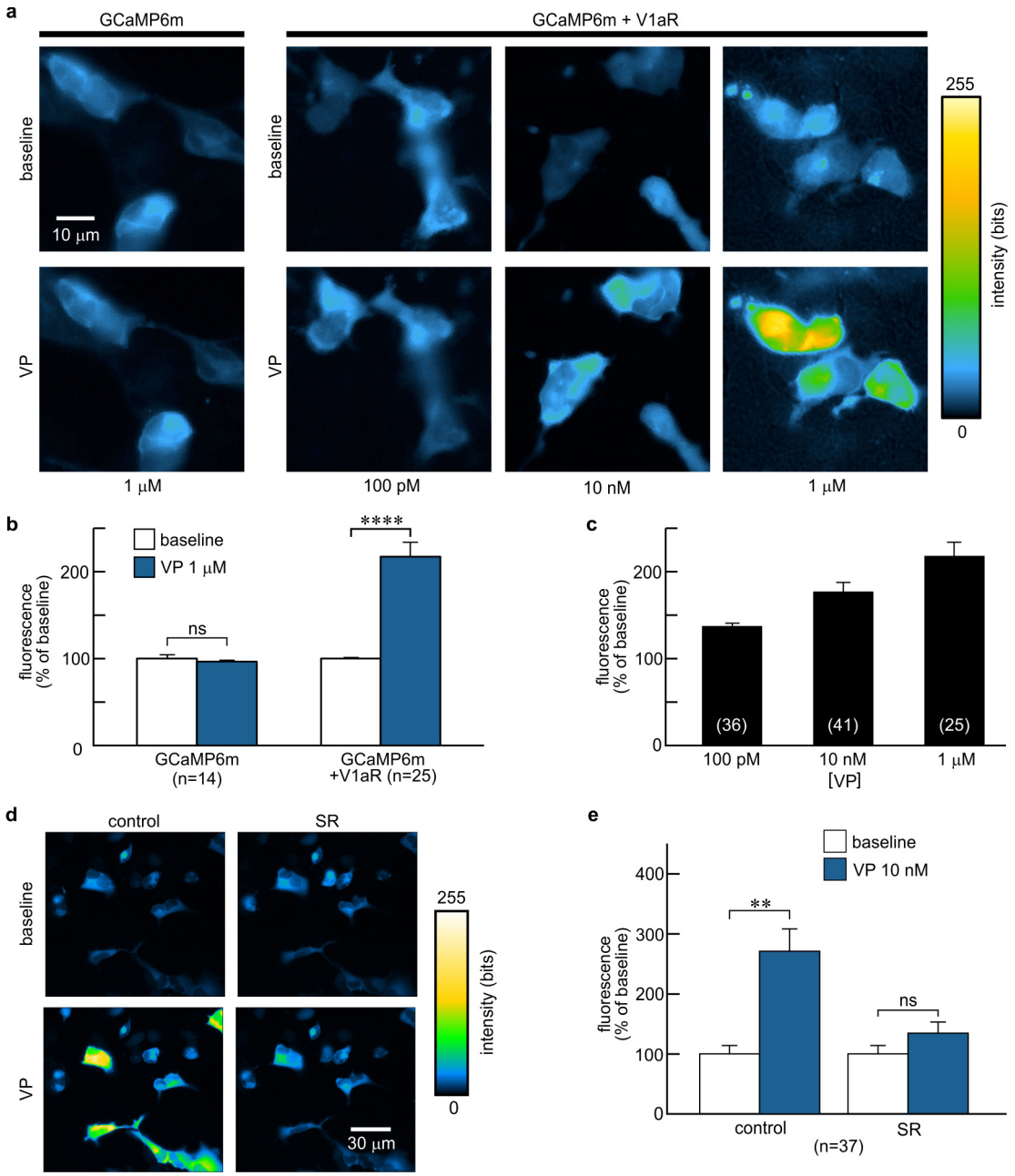

Extended Data Figure 5 | Specificity and calibration of VP sensor cells. **a**, Effects of bath-applied VP (concentrations shown below) on GCaMP6m fluorescence in HEK293 cells transfected with GCaMP6m alone, or co-transfected with GCaMP6m and the human V1aR. Note that VP has no effect in the absence of V1aR, but that dose-dependent increases were observed in the VP sensors co-transfected with GCaMP6m and V1aR. **b**, Bar graphs show mean ± s.e.m. values of fluorescence changes (relative to baseline) caused by 1 μM VP in both types of cells (****$P < 0.0001$; NS, not significant; paired *t*-test; *n* shown in brackets). **c**, Bar graphs show mean ± s.e.m. values of fluorescence (relative to baseline) induced by different concentrations of VP in HEK293 cells transfected with GCaMP6m and V1aR (*n* shown in brackets). **d**, Examples of GCaMP6m fluorescence in VP sensor cells treated with 10 nM VP in the absence (control) or presence of 10 μM SR49059. **e**, Bar graphs show mean ± s.e.m. values of GCaMP6m fluorescence (relative to baseline) induced by 10 nM VP cells in the absence and presence of 10 μM SR49059. Cells were first tested in the presence of SR49059, then SR49059 was washed out and cells were retested in the absence of SR49059 (**$P < 0.01$; two-way RM ANOVA and Holm-Sidak post-hoc test).

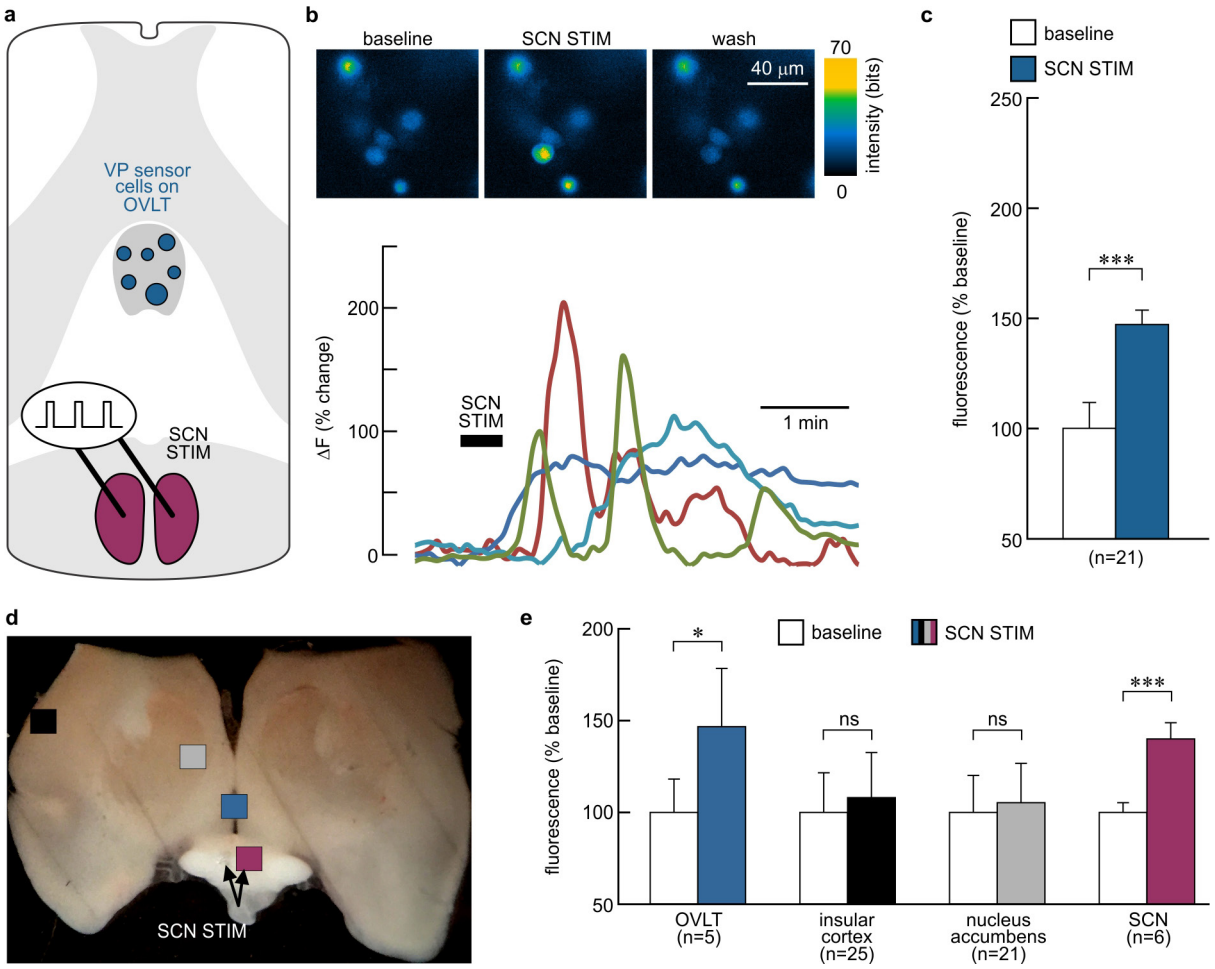

Extended Data Figure 6 | Detection of VP release in slices of mouse and rat hypothalamus. a, Schematic diagram illustrates the configuration of the experiment. HEK293 cells transfected with GCaMP6m and V1aR (VP sensors) were plated over the slice and GCaMP6m fluorescence was imaged over various regions (OVLT illustrated here). **b**, Upper panels show GCaMP6m fluorescence in VP sensors overlying the OVLT before (baseline) and after electrical stimulation of the SCN (SCN STIM; 10 Hz, 30 s) in a slice of mouse hypothalamus. The lower graph plots the time course of changes in fluorescence (ΔF; expressed as per cent of basal fluorescence, % Change) induced by SCN stimulation (bar) in a number of cells. **c**, Bar graphs show mean ± s.e.m. values of fluorescence changes induced by SCN stimulation in slices of mouse hypothalamus relative to baseline (***$P < 0.001$; n shown in brackets, paired t-test). **d**, Photo of a horizontal rat hypothalamic slice depicting four regions where VP sensor fluorescence was measured after SCN stimulation: OVLT (blue), insular cortex (black), nucleus accumbens (grey) and SCN (magenta). **e**, Bar graphs show mean ± s.e.m. GCaMP6m fluorescence before and after SCN stimulation in five representative sensor cells lying over the OVLT, and all cells imaged over the other areas sampled. Note significant release in SCN and OVLT, but not in the other regions (paired t-test used for analysis of OVLT and SCN, and Wilcoxon test used for other regions; *$P < 0.05$; NS, not significant).

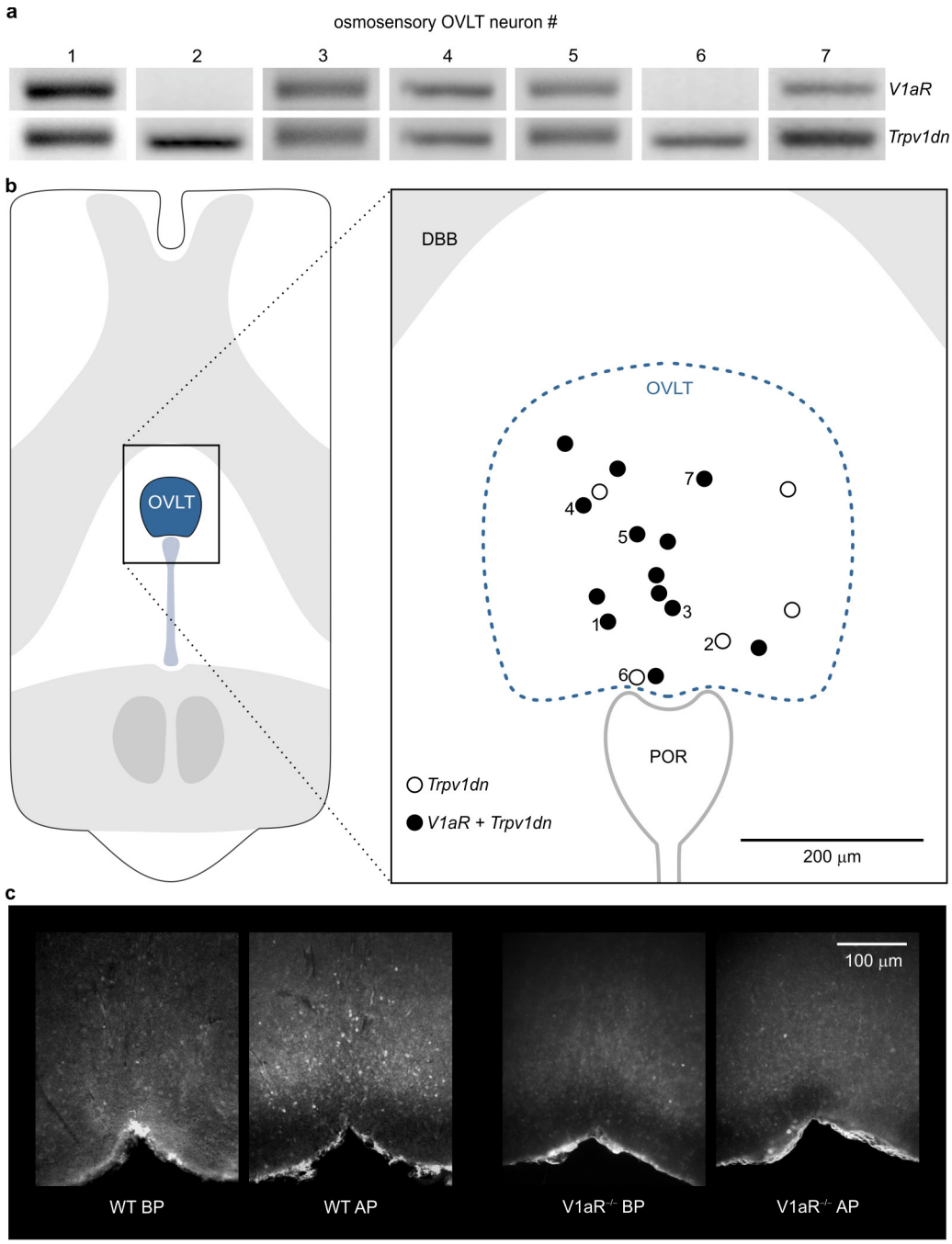

Extended Data Figure 7 | V1aRs are necessary for c-Fos activation during the AP in OVLT neurons. a, Single-cell RT–PCR bands reveal the presence or absence of mRNA encoding VP V1aRs (upper panels) in seven (of 18) individual osmosensory OVLT neurons aspirated via patch pipette in a horizontal slice of rat hypothalamus. The positions of all sampled neurons were measured relative to the rostral part of the preoptic recess (POR) of the third ventricle, and mapped according to ref. 28. Most neurons were sampled in the core of the OVLT. **b**, OVLT neurons were identified as osmosensory neurons by the presence of PCR products reflecting expression of the channel gene *Trpv1dn* (lower panels)[34]. In total, 13 of 18 *Trpv1dn*-positive OVLT neurons (72%) were found to express V1aRs. **c**, Micrographs show expression of immunolabelled c-Fos in the OVLT of wild-type and V1aR$^{-/-}$ mice during the BP and AP. Note that the increase in c-Fos density observed in wild-type mice during the AP is absent in V1aR$^{-/-}$ mice.

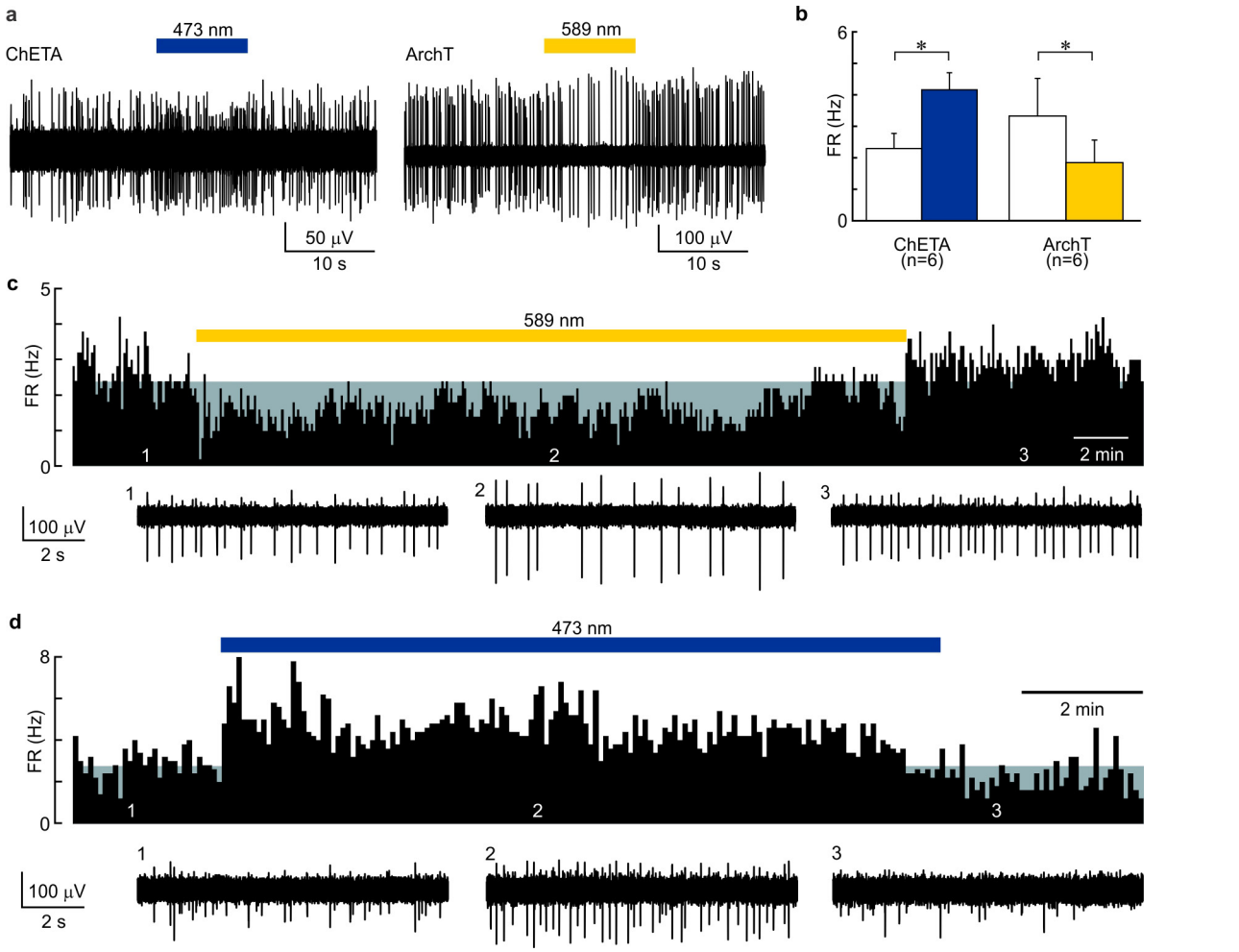

Extended Data Figure 8 | Optogenetic control of SCN VP neurons in ChETA and ArchT mice. a, Cell-attached recordings of spontaneous action potential firing in identified SCN VP neurons in slices prepared from ChETA and ArchT mice. Note how application of blue light (473 nm, blue bar) causes excitation of the ChETA neuron whereas application of yellow light (589 nm, yellow bar) inhibits the ArchT neuron. **b**, Bar graphs show mean ± s.e.m. values of firing rate (FR) measured in SCN VP neurons from both genotypes in the absence (white) and presence of light (blue for ChETA; yellow for ArchT; *n* shown in brackets; $*P < 0.05$; ChETA, paired *t*-test; ArchT, Wilcoxon test). **c**, Upper trace is a rate metre record (5-s bins) showing the effects of prolonged application of yellow light (bar) on firing rate of an SCN VP neuron from an ArchT mouse. Traces below show samples of neuronal activity recorded at the times indicated by the numbers. Note that the inhibitory effect of light on firing rate is sustained for >20 min but diminishes thereafter. **d**, Upper trace is a rate metre record (5-s bins) showing the effects of prolonged application of blue light (bar) on firing rate of an SCN VP neuron from a ChETA mouse. Traces below show samples of neuronal activity recorded at the times indicated by the numbers. Note that the excitatory effect of light on firing rate is sustained for >10 min but declines before the end of the stimulus.

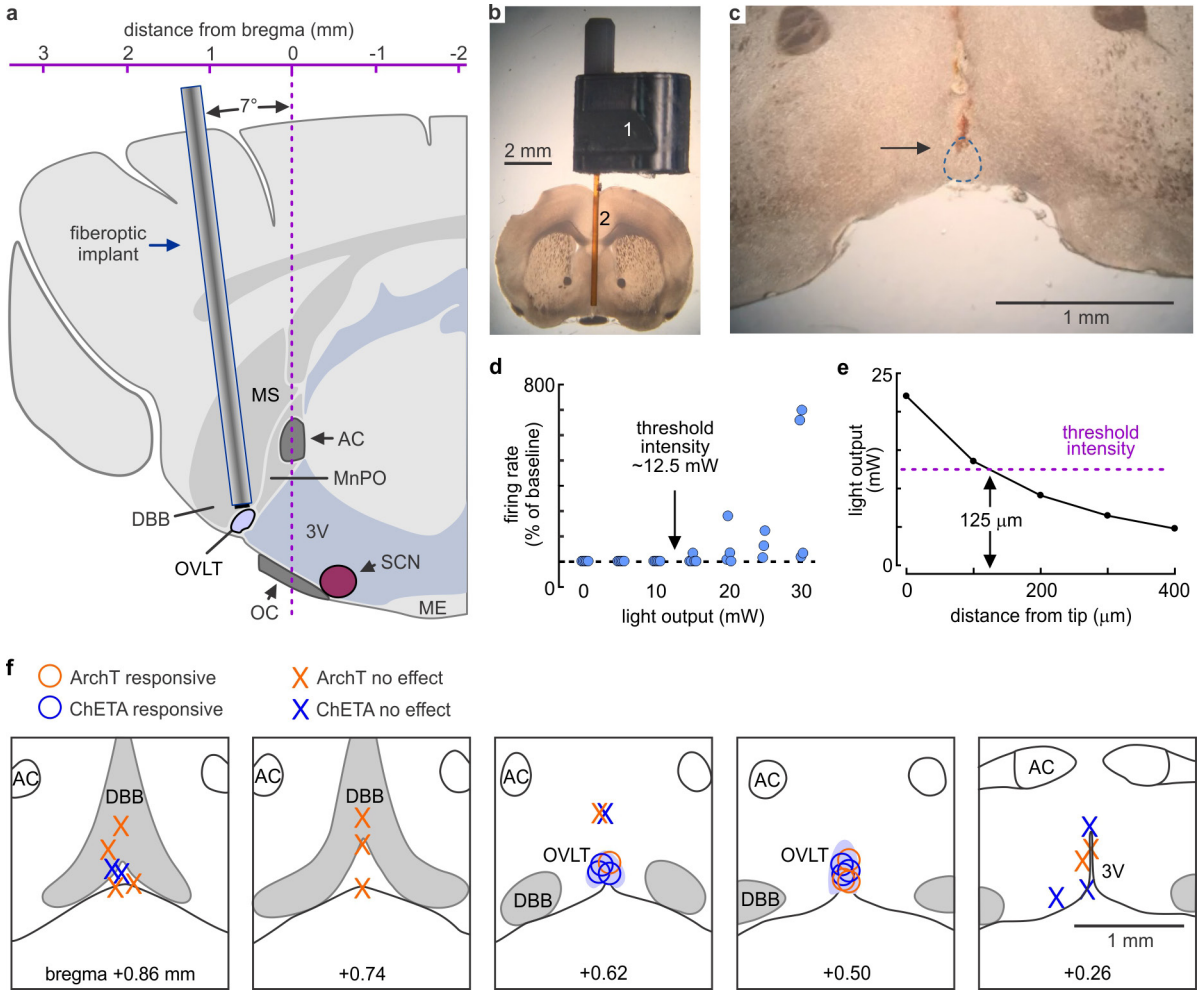

Extended Data Figure 9 | Optogenetic control of OVLT neurons in mice. a, Schematic diagram illustrating midline structures surrounding the mouse OVLT in the sagittal plane. Positions illustrated as described elsewhere[31]. Fibre-optic cannula attached to a slim titanium magnetic receptacle was implanted by insertion at an angle of 7° relative to the vertical plane. **b**, Photograph shows the slim titanium magnetic receptacle and fibre-optic cannula superimposed on a coronal brain slice at the level of the OVLT. **c**, Coronal section from the paraformaldehyde-fixed brain of a mouse that was implanted with a fibre-optic cannula. Inspection of the section revealed that the tip of the cannula had reached the most dorsal part (arrow) of the OVLT (dashed line). **d**, Plot shows the effect of blue light delivered for 1–2 min at different intensities on the firing rate of OVLT neurons in slices from a ChETA mouse *in vitro*. Each dot is a different cell. Note that threshold intensity is ~12.5 mW. **e**, Plot shows theoretical decay of light intensity through brain tissue as a function of distance using our specific parameters and the calculator module provided at http://optogenetic.org. Note that with a light output set at 22 mW (used in our *in vivo* experiments with ChETA mice), light intensity drops below threshold at a distance of ~125 µm from the tip of the fibre-optic probe. **f**, Coronal schematics illustrate implantation sites for all *in vivo* optogenetic experiments determined by post-hoc histological inspection (as in **c**). This image has been adapted from ref. 31. Distance from bregma in the rostro-caudal axis is shown below each panel. Note that experiments were only successful when the tip of the fibre-optic probe was placed directly into or above the OVLT.

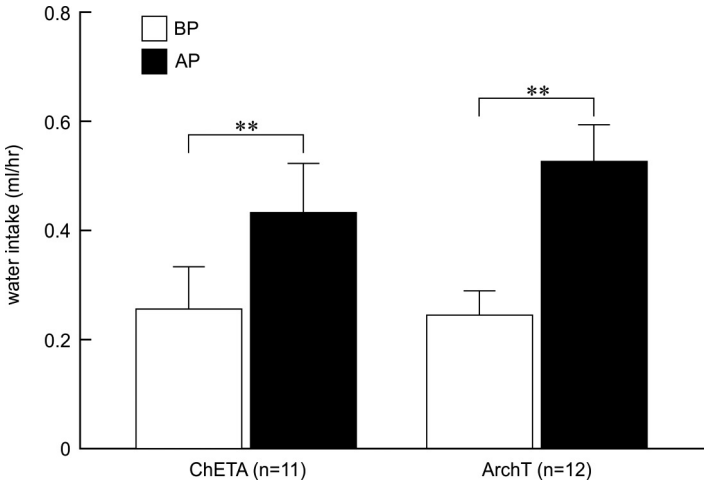

Extended Data Figure 10 | Transgenic ChETA and ArchT mice implanted with fibre-optic cannulae displayed increases in water intake during the AP. Bar graphs show mean ± s.e.m. values of water intake during the BP (ZT19.5–21.5) and AP (ZT21.5–23.5) in groups of ChETA and ArchT mice (paired *t*-test, $^{**}P < 0.01$; *n* shown in brackets).